# Insight into cooling requirements for thermophotovoltaic devices

Bhrigu Rishi Mishra, Alexis Vossier, Inès Revol, Guilhem Almuneau, Rodolphe Vaillon

Solar Energy Materials & Solar Cells 296 (2026) 114023

Contents lists available at ScienceDirect

Solar Energy Materials and Solar Cells

journal homepage: www.elsevier.com/locate/solmat

# Insight into cooling requirements for thermophotovoltaic devices

Bhrigu Rishi Mishra [a], Alexis Vossier [b], Inès Revol [a], Guilhem Almuneau [a], Rodolphe Vaillon [a,*]

[a] LAAS-CNRS, Université de Toulouse, CNRS, Toulouse, France
[b] PROMES-CNRS, Processes, Materials and Solar Energy laboratory, Odeillo, France

ARTICLE INFO

*Keywords:*
Thermophotovoltaics
Cooling
Detailed balance
Pairwise efficiency
Power density
Effective heat transfer coefficient

ABSTRACT

Performance of thermophotovoltaic conversion devices depends on the operating temperature of the cell, and thus on how heat generated in the cell is dissipated. The present research examines the cooling requirements that allow the cell to operate at a specified temperature, based on the parameters influencing electrical power generation. A detailed balance approach and a simple thermal model involving an effective heat transfer coefficient are used. Key parameters, such as emitter temperature, view factor, in-band transmission and out-of-band transmission functions, and external radiative efficiency, are systematically varied to evaluate their influence on pairwise efficiency and power density, and on the required effective heat transfer coefficient to ensure that the cell operates at selected temperatures. Although thermophotovoltaic cells are typically presumed to function at close to ambient, our findings indicate that maintaining this operating temperature necessitates a cooling system with a substantially high effective heat transfer coefficient ($\sim 10^3-10^4$ $Wm^{-2}K^{-1}$). The cooling challenge grows when the cell bandgap diminishes, due to the interplay of rising power density and decreasing pairwise efficiency. The cooling requirements increase with the temperature of the emitter and the view factor. Nevertheless, they can be mitigated by reducing both in-band and out-of-band transmission functions. They are underestimated, and the bandgap optimizing pairwise efficiency or power density is inadequately predicted when the cell is assumed to operate in the radiative limit. These insights into cooling requirements imply that they should be considered from the initial stages of thermophotovoltaic device design.

## 1. Introduction

Thermophotovoltaic (TPV) devices combine a high-temperature thermal emitter and photovoltaic (PV) cells that absorb radiation from the latter for conversion into electrical power [1,2]. Recent experimental works demonstrated TPV devices with pairwise efficiency exceeding 35%. Tervo et al. [3] reported a pairwise efficiency of 38.8% with a single junction GaInAs cell operating at 24 °C with an emitter at 1850 °C. LaPotin et al. [4] demonstrated a TPV device with 41.1% pairwise efficiency using a tandem cell comprising large bandgap semiconductors ($E_g$ = 1.4/1.2 eV). The emitter and cell temperatures were 2400 °C and 60 °C, respectively. Roy-Layinde et al. [5] reported a record pairwise efficiency of 43.8% for a TPV device consisting of a single-junction InGaAsP cell, illuminated by a blackbody emitter at 1435 °C, with the cell maintained near 30 °C. In the above-mentioned experimental studies, the cell is cooled by dissipating heat from its rear (non-illuminated) side to a colder body. This cooling configuration is common in other experimental and most theoretical studies, and is also considered in the present work. In models, heat exchange is typically described using an effective heat transfer coefficient (EHTC), also known as thermal conductance, which quantifies the amount of heat dissipated per unit area of the cell per unit temperature difference between the cell and the cold body. However, in the aforementioned experimental studies, no information is provided about the EHTC or the cooling power required to maintain the cell temperature near ambient.

Previous studies performed detailed balance calculations of TPV devices to evaluate their performance in terms of power density and pairwise efficiency as a function of cell bandgap and emitter temperature [6–8]. In these works, the heat generated in the cell and the required EHTC to maintain the cell operation at room temperature were evaluated. Francoeur et al. [9] investigated how nanoscale-gap spacing affects the thermal management requirements in near-field TPV devices comprising cells made of indium gallium antimonide (InGaSb). Their results showed that a cooling system with an exceptionally high EHTC of $10^5$ $Wm^{-2}K^{-1}$ is required to operate the cell at room temperature with a 20 nm vacuum gap between the cell and the emitter. They also plotted the variations of cell temperature as a function of EHTC and categorized them into three cooling regimes. Within each regime, cell temperatures corresponding to different nanogaps are shown. The

* Corresponding author.
*E-mail address:* rodolphe.vaillon@cnrs.fr (R. Vaillon).

https://doi.org/10.1016/j.solmat.2025.114023
Received 21 July 2025; Received in revised form 13 October 2025; Accepted 15 October 2025

results highlight that for nanogaps below 50 nm, maintaining the cell at ambient temperature requires advanced cooling strategies such as convection with phase change. Dupré et al. [6] optimized the performance of solar thermophotovoltaic systems by accounting for the thermal equilibrium of the TPV cell. Their calculations showed that compared to when the cell temperature is fixed at 300 K, both the maximum power density and the efficiency decrease, and the optimal bandgap for achieving maximum power density shifts to a higher value when the cell temperature is regulated using a cooling system. DeSutter et al. [10] considered a TPV device with a spectrally selective emitter at 2000 K, dissipation of heat to a colder body at 293 K and an EHTC equal to 600 $Wm^{-2}K^{-1}$. The pairwise efficiency was maximized for a GaSb cell using a genetic algorithm by determining the optimal emissivity spectrum for the emitter. Simulation results showed that a maximum pairwise efficiency of 38.8% is obtained when the emitter has a unit emissivity in the energy range of 0.719–0.763 eV and zero elsewhere. It was also observed that reducing the EHTC value while keeping the emitter temperature constant resulted in shortening the width of the optimal emissivity spectrum of the emitter and thus in reducing the pairwise efficiency. Blandre et al. [7] demonstrated a trade-off between conversion efficiency and the operating temperature of a GaSb cell, as a function of the EHTC. They considered 300 K as the lower limit for the cell temperature and also as the condition for maximum efficiency. The study showed that an EHTC of at least 600 $Wm^{-2}K^{-1}$ is required to achieve 90% of the maximum efficiency (i.e., when the cell is at 300 K). Additionally, numerical results indicated that when the EHTC is low, reducing the emitter's emissivity, along with integrating passive radiative cooling, helps reducing the thermal load on the cell and enhances the efficiency. Shan et al. [8] theoretically evaluated the performance of a near-field TPV device comprising a tungsten emitter and an InAs cell, combined with a water flow cooling system. In their analysis, a portion of the TPV devices' power density was allocated to operate the cooling system. The results showed that, at an emitter temperature of 1500 K, a cooling power equal to 1.1% of the maximum electrical power density (277.9 $kWm^{-2}$) was needed to maintain the cell temperature at 325.5 K when operating at the point of maximum power density and slightly less when operating at the maximum pairwise efficiency point.

The previously described theoretical studies incorporate a cooling system in the performance analyses of some specific TPV devices. Since these works are limited to particular cases, they do not provide a generalized framework or a criterion to select a suitable cooling system based on the required EHTC under varying conditions. This highlights a gap in the literature where a broader, more systematic understanding of cooling requirements in TPV devices is lacking. In this work, we address this gap by quantifying the cooling requirements in terms of the EHTC as a function of the bandgap of the cell across a wide range of operating scenarios. We also evaluate the change in power density, pairwise efficiency, and effective heat transfer coefficient when the cell does not operate at its radiative limit. The aim is to provide insightful information that can help design TPV devices with suitable thermal management under more generalized and practical conditions.

## 2. Methods

In this work, the cooling requirements are theoretically studied in terms of the EHTC of a cooling system over a range of cell bandgap. The performance metrics of TPV devices, such as power density and pairwise efficiency, are also evaluated. Our 1D thermal model considers a TPV device with a cold body at a temperature $T_{cold}$ to which heat generated in the cell is dissipated (see a schematic in Fig. 1).

Considering a unit area of the emitter and the cell, the energy balance equation for the cell is

$$q_{abs} - p_{out}(T_c) - h_{eff}\,(T_c - T_{cold}) = 0, \tag{1}$$

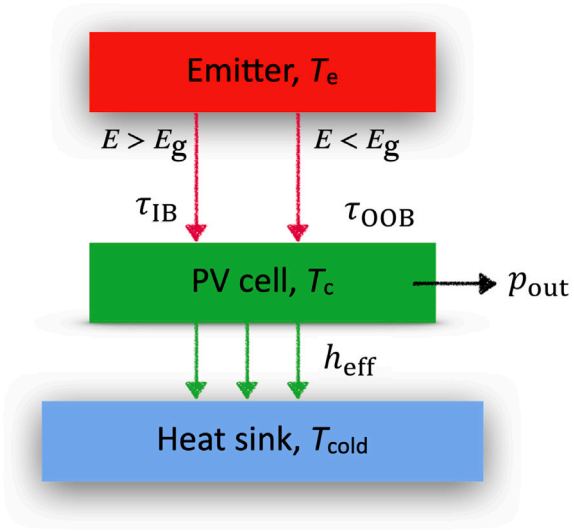


**Fig. 1.** Schematic of a TPV device composed of an emitter, a TPV cell, and a cooling system to dissipate the heat generated in the cell.

where, $q_{abs}$, $p_{out}$, $h_{eff}$, $T_c$, and $T_{cold}$ are the net heat radiation power density absorbed by the cell, the generated electrical power density, the effective heat transfer coefficient, the temperature of the cell, and the temperature of the cold body to which heat generated in the cell is dissipated, respectively. The pairwise efficiency of the TPV device is calculated as

$$\eta_{pair} = \frac{p_{out}}{q_{abs}}. \tag{2}$$

The net heat radiation power density absorbed by the cell is calculated as

$$q_{abs} = VF\left(\int_0^{E_g} \tau_{OOB}(E)\; E\; b(E, V=0, T_e)\; dE + \int_{E_g}^{\infty} \tau_{IB}(E)\; E\; b(E, V=0, T_e)\; dE\right), \tag{3}$$

where, $VF$, $E$, $E_g$, $T_e$, $b(E,V,T)(= \frac{2\pi E^2}{h^3c^2}\frac{1}{\exp(\frac{E-qV}{kT})-1}$, $k$ being the Boltzmann constant and $V$ the applied voltage), $\tau_{OOB}$, and $\tau_{IB}$ are the view factor, photon energy, bandgap of the cell, emitter temperature, spectral photon flux of a blackbody with chemical potential $V$, out-of-band (OOB) transmission function, and in-band (IB) transmission function between the emitter and the cell, respectively. It is worth noting that the transmission function is also called "effective emittance of the emitter–cell pair" [1,11]. It accounts for multiple reflections of photons between the two surfaces.

The output power density of the TPV device is calculated using the detailed balance formalism [12,13]. The electrical power density is expressed as

$$p_{out} = \mathrm{Max}\left[(J_{sc} - J_r(V)) \cdot V\right] \tag{4}$$

where $J_{sc}$ and $J_r(V)$ are the photogenerated current (also the short-circuit current) and the recombination current (current loss resulting from the recombinations), respectively, given by

$$J_{sc} = VF\; q \int_{E_g}^{\infty} \tau_{IB}(E)\; E\; b(E, V=0, T_e)\; dE, \tag{5}$$

$$J_r = \frac{f_g}{ERE}\, q \int_{E_g}^{\infty} E\; b(E, V, T_c)\; dE, \tag{6}$$

The voltage at which power is maximum is found by varying the voltage between 0 and the open-circuit voltage

$$V_{oc} = \frac{kT_c}{q}\left(\ln\frac{J_{sc}}{J_r} + 1\right). \tag{7}$$

**Table 1**
Values of the physical parameters used in the base configuration and in other ones.

| Physical parameter | Base configuration | Other configurations |
|---|---|---|
| Cold body temperature ($T_{cold}$) | 25 °C | 25 °C |
| Cell temperature ($T_c$) | 30, 50, 80 °C | 50 °C |
| Emitter temperature ($T_e$) | 1500 °C | 1800, 1200 °C |
| View factor ($VF$) | 1 | 0.5, 0.1 |
| In-band transmission function ($\tau_{IB}$) | 1 | 0.8, 0.6 |
| Out-of-band transmission function ($\tau_{OOB}$) | 0.02 | 0.1, 0.01 |
| External Radiative Efficiency ($ERE$) | 1 | $10^{-1}$, $10^{-3}$, $10^{-6}$ |

Here, the factor $f_g$ is equal to 1 (applying to a monofacial cell, opaque at the back, allowing photon recycling). $ERE$ is the external radiative efficiency, which is the ratio of radiative to total recombination current densities [12,13]. An ERE of 1 means that the cell operates at the radiative limit.

In all subsequent subsections, cooling requirements are quantified in terms of the EHTC needed to operate the TPV cell at a specified temperature ($T_c$). Subsequently, following the calculation of power density and pairwise efficiency, Eq. (1) is used to determine the effective heat transfer coefficient.

## 3. Results and discussion

Unless specified otherwise, the base configuration is with the emitter temperature at 1500 °C, a view factor equal to 1, the in-band and the out-of-band transmission functions equal to 1 and 0.02, respectively, the cell operating at the radiative limit ($ERE = 1$), and the cold body temperature equal to 25 °C. Here, it is assumed that the available cold body temperature is that of the ambient (i.e., there is no colder – free – source available nearby). In the base configuration, three target cell temperatures are selected: 30, 50, and 80 °C. Cooling requirements are quantified as a function of the cell bandgap. The base configuration is analyzed first. Then, one parameter is changed at a time in the subsequent subsections (see Table 1).

### 3.1. Analysis in the base configuration

It is well known that in the radiative limit, both power density and pairwise efficiency decrease with the cell temperature [14]. This is observed in Figs. 2(a) and 2(b). The maximum pairwise efficiency and power density decrease from 56.3% to 53.4% and 18.6 $Wcm^{-2}$ to 17.7 $Wcm^{-2}$, when the cell temperature increases from 30 °C to 80 °C, respectively. The EHTC required to ensure a specified cell temperature is shown in Fig. 2(c). As the bandgap decreases, the EHTC rises sharply. For example, when the cell temperature is equal to 30 °C, the required EHTC is $1.59\times10^4$ $Wm^{-2}K^{-1}$ (also read as 1.59 $Wcm^{-2}K^{-1}$) for a bandgap of 0.7 eV, and rises to $7.13\times10^4$ $Wm^{-2}K^{-1}$ for a bandgap of 0.2 eV. This is explained by the variation in heat power density generated in the cell, which is proportional to power density and inversely proportional to pairwise efficiency [11]. Of course, an increase in the target cell temperature results in a lower cooling need, thereby decreasing the EHTC.

For the sake of illustration, a color scale is shown in Fig. 2(d) to link ranges of EHTC values with existing cooling methods. This scale, already used in Ref. [15], defines ranges with limits that are not strictly defined. For example, to operate the cell with a bandgap of 0.7 eV at a temperature close to ambient, forced cooling using water microchannels is required. Increasing the operating temperature of a TPV cell to 50 °C reduces the EHTC to $0.327\times10^4$ $Wm^{-2}K^{-1}$, and thus a "water channel" cooling system is suitable.

In Fig. 2(e), pairwise efficiency is plotted as a function of power density, for each of the three target cell temperatures. One curve provides these two metrics as a function of cell bandgap, which increases along the curve from the lower right to the lower left. Along the same curve, the value of the EHTC required to have the cell operate at a given temperature is provided using a color scale. This figure directly shows that when the cell operates at 30 °C, the bandgap at which power density is maximum (0.32 eV) is very different from that at which efficiency is maximum (0.83 eV) [11]. At the bandgap at which power density is maximum (18.6 $Wcm^{-2}$), pairwise efficiency is equal to 41.3%. This efficiency reaches a peak value of 56.3%, but with a reduction in power density down to 6.6 $Wcm^{-2}$. The decline in EHTC as bandgap increases is visible. This relates to the simultaneous reduction in power density and enhancement in efficiency, both resulting in a decrease in heat generated within the cell. As a result, all three curves in Fig. 2(e) clearly indicate that operating the TPV device at the maximum pairwise efficiency point (MPEP) necessitates a lower EHTC compared to operating it at the maximum power density point (MPDP).

The main insight of this subsection is that low-bandgap cells correlate with larger cooling requirements (larger EHTC), especially for operating the cells near ambient temperature (30 °C). This observation applies to each configuration examined in this study. This is illustrated by the fact that on all efficiency vs power density curves, the EHTC always increases from the highest bandgap (lower-left) point to the lowest bandgap (lower-right) point.

In the following sections, the target cell temperature is prescribed at 50 °C. One input parameter changes at a time (i.e. all other parameters are the same as those used in the base configuration). For ease of comparison, the EHTC scale will be kept consistent from the next subsection onward.

### 3.2. Impact of the emitter temperature

Pairwise efficiency vs power density is plotted in Fig. 3 for the emitter temperatures of 1200, 1500, and 1800 °C. The figure shows that power density increases substantially with rising emitter temperature. This is explained by the fact that radiation power originating from the emitter increases with the fourth power of its temperature. The emission spectrum is also modified, with a shift of its peak toward a larger photon energy. This results in a larger fraction of the emitted energy spectrum falling within the in-band spectral region, which contributes to the rise in power density. Correlatively, the lower out-of-band fraction of the total power contributes to the increase in pairwise efficiency.

In terms of cooling requirements, the EHTC logically rises significantly with the emitter temperature, in particular close to the bandgaps where power density is maximum (MPDP). As the emitter temperature increases from 1200 to 1800 °C, the bandgap at which power density is maximum increases from 0.26 eV to 0.37 eV, with a corresponding power density growing drastically from 8.1 to 35.8 $Wcm^{-2}$. The EHTC required to maintain the cell at 50 °C rises significantly from $0.545\times10^4$ to $1.96\times10^4$ $Wm^{-2}K^{-1}$. Similarly, the bandgap at which pairwise efficiency is maximum shifts from 0.69 eV to 0.96 eV, with the pairwise efficiency value rising from 51.46% to 57.82%. The EHTC at the maximum pairwise efficiency point rises considerably from $0.064\times10^4$ to $0.382\times10^4$ $Wm^{-2}K^{-1}$.

The main insight of this subsection is that increasing the emitter temperature implies significantly larger cooling requirements, which are particularly high for bandgaps close to the maximum power density point.

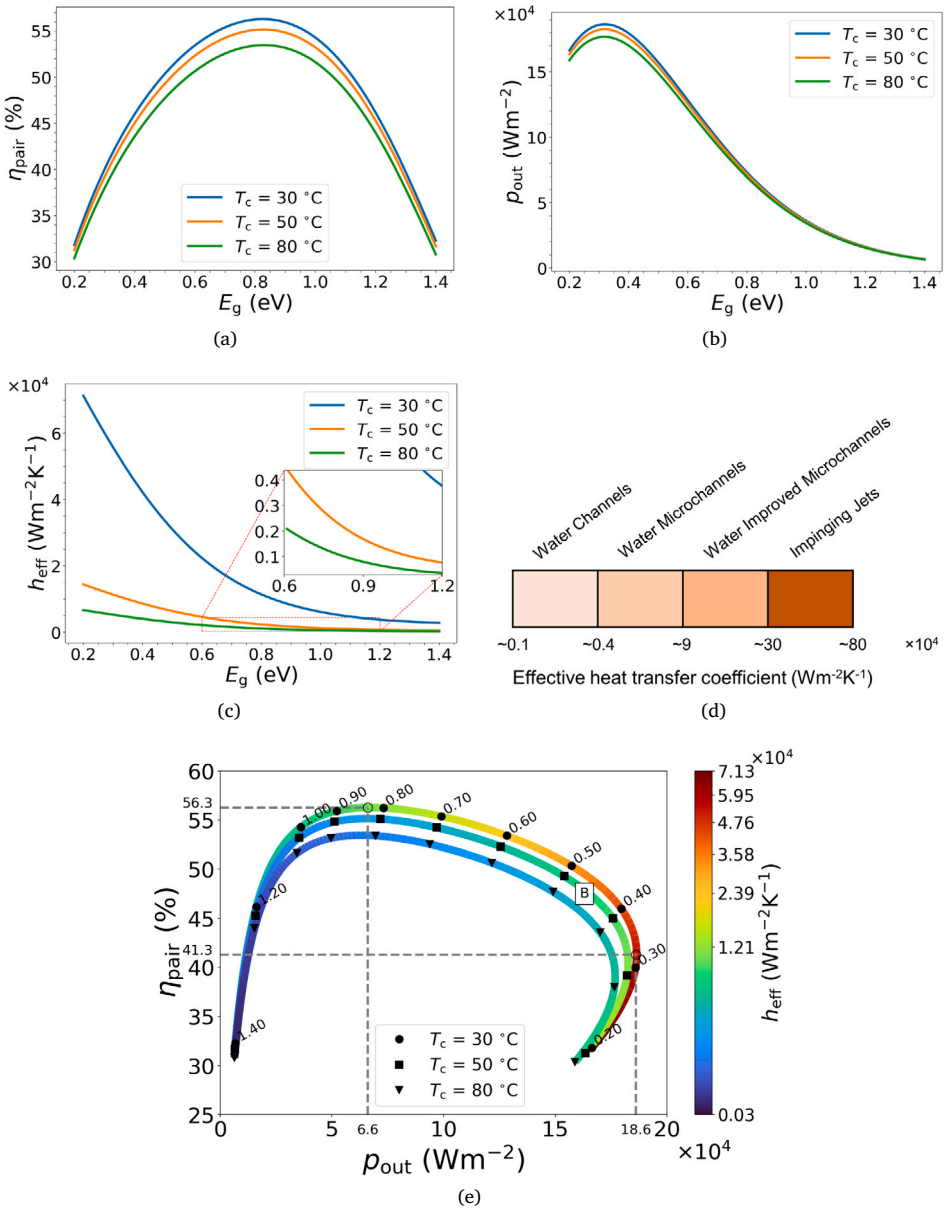


**Fig. 2.** (a) Pairwise efficiency ($\eta_{pair}$), (b) power density ($p_{out}$), and (c) effective heat transfer coefficient ($h_{eff}$) for three cell temperatures ($T_c$) as a function of bandgap ($E_g$) of the cell. (d) Color bar indicating the range of EHTC corresponding to different types of cooling methods, inspired from Ref. [15]. (e) Pairwise efficiency vs power density curves. A colormap is used to show the variations in EHTC along these curves. The bandgap is indicated along the curve. The base configuration is highlighted using the letter 'B' in a square box.

### 3.3. Impact of the view factor

In this section, the impact of the view factor, which quantifies the fraction of radiation power leaving the emitter that is incident on the cell, is analyzed for three values: 0.1, 0.5, and 1. The radiation power incident on the cell increases in proportion to the view factor, its spectrum remaining the same. Thus, the view factor plays the same role as the concentration factor in solar photovoltaics. As expected, a larger view factor causes a higher power density, as depicted in Fig. 4. Pairwise efficiency rises more slowly than power density as the view factor is increased from 0.1 to 1. This is because the power absorbed by the cell is directly proportional to the view factor, while the electrical power density does not scale linearly with it. As a result, pairwise efficiency, defined as the ratio of electrical power density to the absorbed radiation power density, increases more slowly than the power density when the view factor rises.

Fig. 4 shows that when the view factor increases from 0.1 to 1, the bandgap at the maximum pairwise efficiency point shifts from 0.88 eV to 0.83 eV, with the corresponding pairwise efficiency increasing slightly from 49.85% to 55.15%. The corresponding power density rises substantially from 0.50 Wcm$^{-2}$ to 6.5 Wcm$^{-2}$. Accordingly, the EHTC required to operate the cell at 50 °C increases by a factor ~10, from 0.020×10$^4$ Wm$^{-2}$K$^{-1}$ to 0.211×10$^4$ Wm$^{-2}$K$^{-1}$. Similarly, the bandgap at the MPDP slightly decreases from 0.37 eV to 0.32 eV, the maximum power density increasing by a factor 12.9 from 1.42 Wcm$^{-2}$ to 18.26 Wcm$^{-2}$. The corresponding pairwise efficiency rises from 34.33% to 40.50%. Again, the EHTC increases by a factor ~10 from 0.109×10$^4$ Wm$^{-2}$K$^{-1}$ to 1.07×10$^4$ Wm$^{-2}$K$^{-1}$.

It is worth having in mind that in experimental works, the view factor is most of the time smaller than 0.4 [3–5,11]. The main insight of this subsection is that while increasing the view factor to values nearer

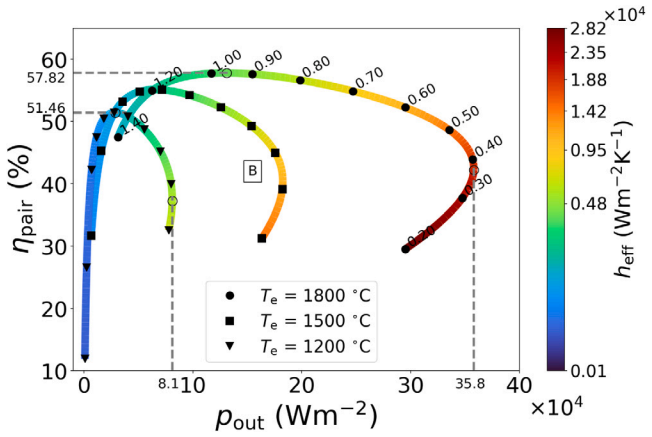


**Fig. 3.** Pairwise efficiency vs power density for three values of the emitter temperature. All other parameters are those of the base configuration highlighted using the letter 'B' in a square box.

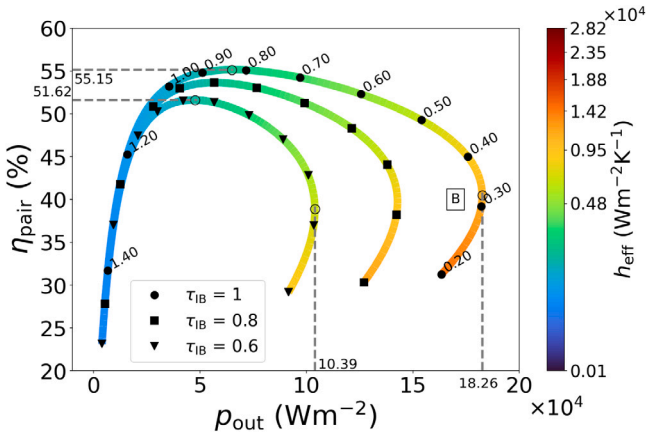


**Fig. 5.** Pairwise efficiency vs power density for three values of the in-band transmission function. All other parameters are those of the base configuration highlighted using the letter 'B' in a square box.

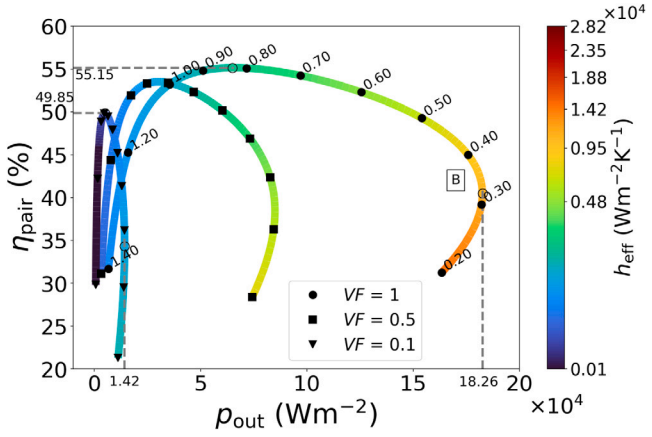


**Fig. 4.** Pairwise efficiency vs power density for three values of the view factor. All other parameters are those of the base configuration highlighted using the letter 'B' in a square box.

to unity will provide the anticipated positive effects on power density and pairwise efficiency, and the cooling requirements will also rise in a similar proportion.

### 3.4. Impact of the in-band and out-of-band transmission functions

While varying the view factor has a spectrally uniform impact, changing the transmission functions has spectrally selective effects. The in-band transmission function affects the radiation absorbed by the cell that contributes to electrical power generation, whereas the out-of-band transmission function influences the absorbed radiation power solely contributing to heating the cell. As a consequence, reducing in-band radiation exchange has a more pronounced effect on power density than on pairwise efficiency as shown in Fig. 5. When the in-band transmission factor decreases from 1 to 0.6, the maximum power density and the required EHTC vary from 18.26 Wcm$^{-2}$ to 10.40 Wcm$^{-2}$ and from 1.07×10$^4$ Wm$^{-2}$K$^{-1}$ to 0.653×10$^4$ Wm$^{-2}$K$^{-1}$, respectively. Similarly, the maximum pairwise efficiency and required EHTC diminish slightly from 55.15% to 51.62% and from 0.211×10$^4$ Wm$^{-2}$K$^{-1}$ to 0.178×10$^4$ Wm$^{-2}$K$^{-1}$, respectively. When the in-band transmission function decreases to 0.6, Fig. 5 shows that the efficiency peak shifts from 0.83 eV to 0.76 eV, but the efficiency at these two bandgap values is almost identical (difference of only 0.3 percentage points). In contrast, the bandgap corresponding to maximum power density remains nearly unchanged, with only a slight shift from 0.32 eV to 0.33 eV.

Fig. 6 shows the pairwise efficiency vs power density curves when the out-of-band transmission function varies from 0.1 to 0.01. Since the in-band transmission function is unity in all three cases shown in Fig. 6, the absorbed photon flux contributing to electrical power generation remains the same, resulting in a constant power density for a given bandgap. For low-bandgap cells (< 0.4 eV), pairwise efficiency and EHTC values are similar for all three cases. A non-optimal spectral selectivity ($\tau_{OOB}$ = 0.1) causes the pairwise efficiency to drop significantly for bandgaps larger than around 0.6 eV. The difference in pairwise efficiency and EHTC between $\tau_{OOB}$ = 0.02 and $\tau_{OOB}$ = 0.01 is negligible for bandgaps below 0.6 eV. However, for bandgaps greater than 0.6 eV, a noticeable divergence emerges for pairwise efficiency, as shown in Fig. 6. When the out-of-band transmission function is equal to 0.1, a maximum pairwise efficiency of 47.18% is found at a bandgap of 0.6 eV, with the corresponding power density and EHTC equal to 12.56 Wcm$^{-2}$ and 0.562×10$^4$ Wm$^{-2}$K$^{-1}$, respectively. By reducing the out-of-band transmission function to 0.01, the maximum pairwise efficiency is increased to 57.83%, with the corresponding bandgap shifting to a much higher value (0.93 eV). The power density and the EHTC at this bandgap are reduced to 4.60 Wcm$^{-2}$ and 0.134×10$^4$ Wm$^{-2}$K$^{-1}$, respectively. Thus, for bandgaps significantly larger than that of the maximum power density point, reducing the out-of-band transmission function enhances the pairwise efficiency and reduces the cooling requirements. It is clearly visible in Fig. 6 that even if one selects a 0.6 eV cell to achieve a higher power (12.56 Wcm$^{-2}$), reducing the out-of-band transmission from 0.1 to 0.01 increases the pairwise efficiency from 47.18% to 53.03%, and as a consequence, the EHTC drops to a lower value of 0.445×10$^4$ Wm$^{-2}$K$^{-1}$.

The main insight of this subsection is that the in-band transmission function has a significant impact on cooling requirements for bandgaps smaller than that of the maximum pairwise efficiency point, while the out-of-band transmission function has a significant impact for bandgaps larger than that of the maximum power density point.

### 3.5. Impact of the external radiative efficiency

The impact of non-radiative recombination losses is analyzed. In addition to an ERE of 1 (radiative limit), three values of the ERE ($10^{-1}$, $10^{-3}$, and $10^{-6}$), typically found for solar PV cells [13,16], are considered. It is worth noting that the ERE of the InGaAs TPV cell of Ref. [5], calculated using the formula given in Ref. [16], is 0.082. The physical implication of the decrease in ERE is that non-radiative

**Table 2**
Pairwise efficiency ($\eta_{pair}$), power density ($p_{out}$), and effective heat transfer coefficient ($h_{eff}$) corresponding to bandgaps ($E_g$) at which power density is maximum (MPDP) and pairwise efficiency is maximum (MPEP) for three values of the external radiative efficiency ($ERE$).

| | $E_g$ (eV) | | | | $\eta_{pair}$ (%) | | | | $p_{out}$ (Wcm$^{-2}$) | | | | $h_{eff} \times 10^4$ (Wm$^{-2}$K$^{-1}$) | | | |
|---|---|---|---|---|---|---|---|---|---|---|---|---|---|---|---|---|
| $ERE$ | 1 | $10^{-1}$ | $10^{-3}$ | $10^{-6}$ | 1 | $10^{-1}$ | $10^{-3}$ | $10^{-6}$ | 1 | $10^{-1}$ | $10^{-3}$ | $10^{-6}$ | 1 | $10^{-1}$ | $10^{-3}$ | $10^{-6}$ |
| MPDP | 0.32 | 0.37 | 0.49 | 0.70 | 40.49 | 34.33 | 25.15 | 17.11 | 18.26 | 14.20 | 8.05 | 3.06 | 1.07 | 1.09 | 0.958 | 0.592 |
| MPEP | 0.83 | 0.88 | 0.97 | 1.09 | 55.15 | 49.84 | 40.20 | 27.83 | 6.50 | 4.96 | 2.96 | 1.37 | 0.211 | 0.199 | 0.176 | 0.142 |

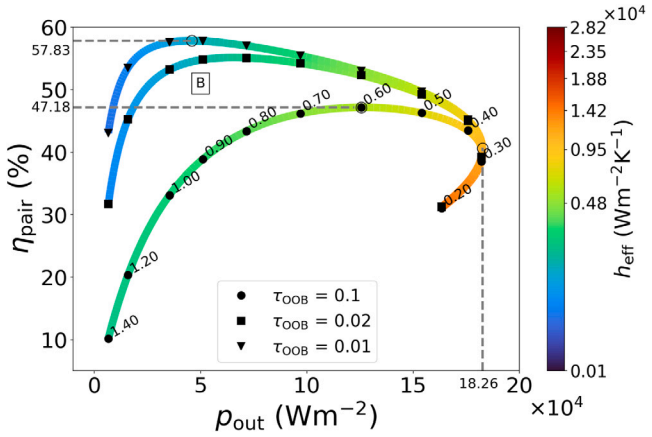


**Fig. 6.** Pairwise efficiency vs power density for three values of the out-of-band transmission function. All other parameters are those of the base configuration highlighted using the letter 'B' in a square box.

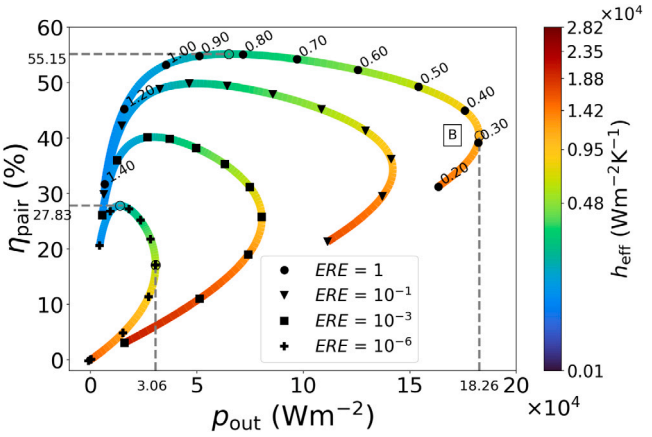


**Fig. 7.** Pairwise efficiency vs power density for four values of the ERE. All other parameters are those of the base configuration highlighted using the letter 'B' in a square box.

recombination becomes dominant: when the ERE decreases from 1 to $10^{-3}$, the recombination current is 1000 times larger, with only 0.1% of it caused by radiative processes and the rest by non-radiative processes [13]. When a cell works at the radiative limit ($ERE = 1$), the performance metrics are maximum. As the ERE is reduced below 1, the performance metrics reduce abruptly, as shown in Fig. 7. For instance, when the ERE is changed from 1 to $10^{-6}$, the absolute reduction in maximum pairwise efficiency and maximum power density is 27.32% and 15.20 Wcm$^{-2}$, respectively.

The values of bandgap, pairwise efficiency, power density, and EHTC at the maximum power density and maximum pairwise efficiency points are given in Table 2. The bandgaps at these specific points are shifted to larger values. This shift in bandgap at these points results in a slight reduction of the EHTC required to operate the cell at the target temperature (50 °C). This behavior is explained by a larger reduction in power density than in pairwise efficiency (reminding that heat power density generated in the cell is proportional to power density and inversely proportional to pairwise efficiency [11]). However, it is worth noting that for a particular bandgap, the EHTC rises when the ERE is decreased. For example, for a bandgap of 0.74 eV (InGaAs), the EHTC increases from $0.285\times10^4$ Wm$^{-2}$K$^{-1}$ to $0.399\times10^4$ Wm$^{-2}$K$^{-1}$, when the ERE decreases from 1 to $10^{-3}$. This time, this behavior is explained by a larger decrease in efficiency than in power density. For an ERE of $10^{-6}$, power density and pairwise efficiency are equal to zero for bandgaps less than 0.4 eV. For this reason, all the points with bandgap less than 0.4 eV are overlapped at (0,0) in Fig. 7.

The main insight of this subsection is that non-radiative recombination losses logically reduce pairwise efficiency and power density. The EHTC required to maintain the cell temperature becomes significantly larger for a selected bandgap. Furthermore, when the cell does not operate at the radiative limit, the bandgaps at the maximum pairwise efficiency and power density points shift to a higher value, while the EHTC decreases slightly. These observations highlight the importance of incorporating the actual ERE of the cell when designing a TPV device. If the ERE is not accounted for, the calculations may incorrectly predict the bandgap at which the pairwise efficiency and power density are maximized for a given emitter temperature and the associated required EHTC to ensure that the cell operates at the selected temperature.

### 3.6. Trends and additional insights on cooling requirements

In previous subsections, key parameters of TPV devices have been varied, and the EHTC required to operate the cell at a target temperature has been calculated. The results suggest that the EHTC is one of the most important parameters that should be considered while designing a TPV device. Most values of the EHTC calculated in the present work are quite high. For example, they are ranging from $0.662\times10^4$ Wm$^{-2}$K$^{-1}$ to $7.13\times10^4$ Wm$^{-2}$K$^{-1}$ to maintain the cell temperature between 30 and 80 °C with a cold body at 25 °C and emitter at 1500 °C, assuming a cell bandgap equal to 0.2 eV. If the cooling is not appropriate, the cell temperature may, in some extreme cases, reach its melting point [10]. In this subsection, a summary of previous results is presented in Fig. 8 by comparing the power density, pairwise efficiency, and EHTC values of all the considered parameters for three bandgap values, namely 0.5 eV (InGaAsSb), 0.74 eV (InGaAs, GaSb), and 1.1 eV (Si). The base configuration (with $T_c$ = 50°C) is also highlighted in each case. The figure helps to visualize simultaneously the sensitivity of the power density, pairwise efficiency, and EHTC to the selected key parameters.

The scenario involving the lowest bandgap cell leads to the largest values of power density but also requires the highest values of EHTC. In particular, it is highly ambitious to operate a 0.5 eV cell close to the ambient temperature and with an emitter temperature above 1500 °C. More generally, the figure shows that the EHTC and power density values scale hierarchically as a function of bandgap in all cases shown in Fig. 8: $p_{out}$(0.5 eV) > $p_{out}$(0.74 eV) > $p_{out}$(1.1 eV) and $h_{eff}$(0.5 eV) > $h_{eff}$(0.74 eV) > $h_{eff}$(1.1 eV). This is not the case for pairwise efficiency. The InGaAs cell has the largest efficiency values for any cell temperature, view factor and in-band transmission function considered in the present analysis. Silicon is a slightly better choice when the emitter temperature is equal to 1800°C. The devices with

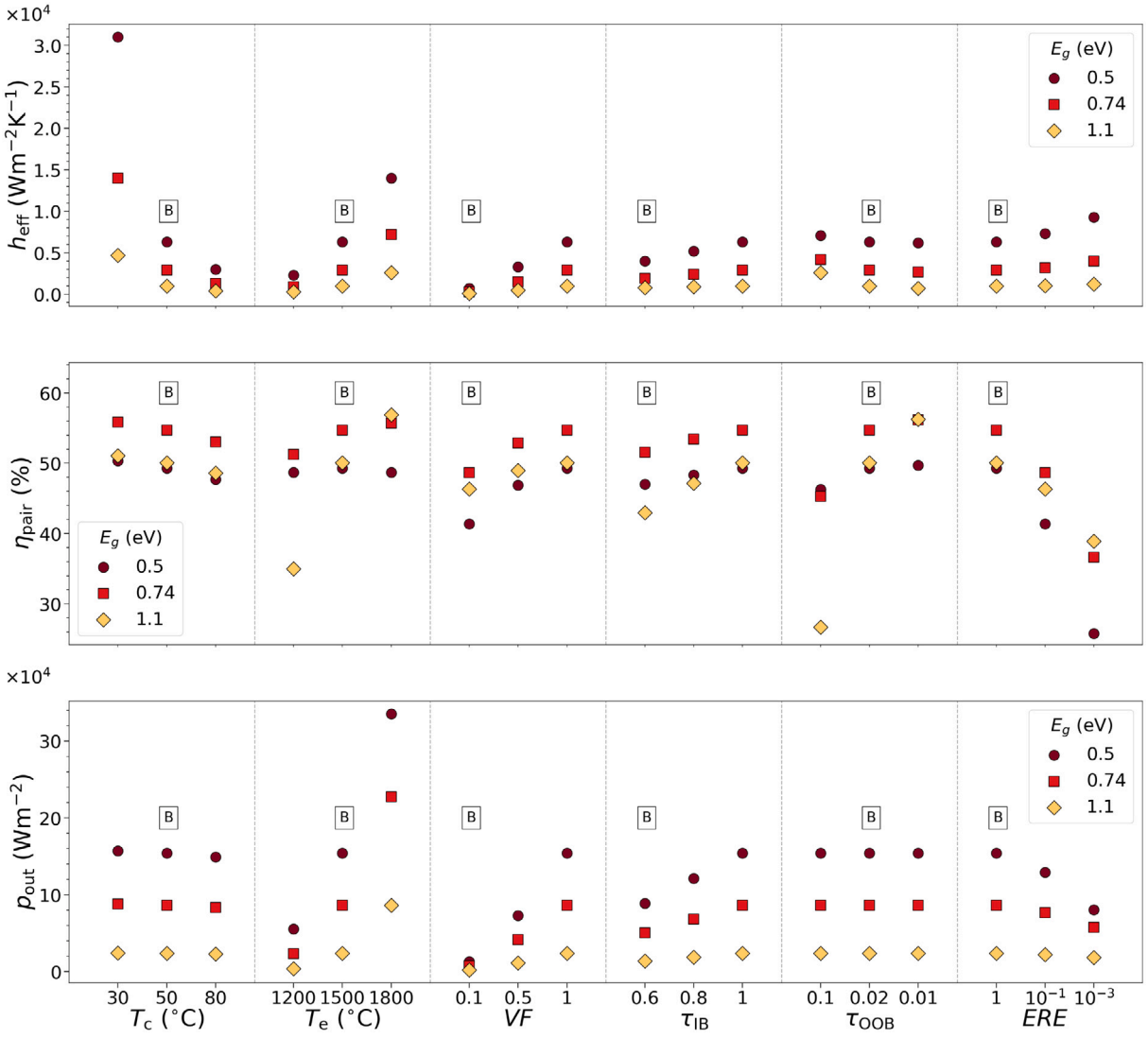


**Fig. 8.** Trends in EHTC, pairwise efficiency, and power density for three bandgap values as a function of operating conditions and design parameters. The base configuration is highlighted using the letter 'B' in a square box.

InGaAs and Si cells have equal pairwise efficiencies when the out-of-band transmission is 0.01. However, when the out-of-band transmission is 10%, the device with the silicon cell has by far the smallest efficiency. When the cells operate in the radiative limit or close ($ERE = 1$ or 0.1), the best efficiency is reached with the InGaAs cell. However, the Si cell exhibits the best efficiency when the ERE value drops to $10^{-3}$. It is important to note that the observations made for efficiency could be different for other emitter temperatures.

Although challenges in cooling requirements are partially relaxed for larger bandgap cells, they are still not negligible. The sensitivity of the EHTC to the view factor, the in-band and out-of-band transmission functions, is moderate for medium (0.74 eV) to high (1.1 eV) bandgap cells. The cooling requirements are quite reduced when the cell is allowed to operate at a temperature significantly above ambient and when the emitter temperature is below 1500 °C. However, to operate the cell close to ambient temperature, illuminated by an emitter at high emitter temperature (>1500 °C), and with significant non-radiative recombination losses ($ERE \ll 1$), the required EHTC rises substantially. These observations highlight that parameters such as emitter temperature ($T_e$), cell operating temperature ($T_c$), bandgap ($E_g$), external radiative efficiency ($ERE$), as well as spectral radiation exchange conditions ($\tau_{IB}$ and $\tau_{OOB}$), are critical parameters to be accounted for in the determination of cooling requirements for TPV devices.

## 4. Conclusion

Using a detailed balance analysis, we have determined the necessary cooling requirements for operating TPV cells at specified temperatures, taking into account the multiple factors influencing the performance of a TPV device. The main conclusion of this analysis, supported by pairwise efficiency–power density curves as a function of the cell bandgap, is that the cooling requirements are usually substantial (EHTC $\sim 10^3 - 10^4$ $Wm^{-2}K^{-1}$), and always get larger as the cell bandgap decreases. Also, the analyses conducted parameter by parameter suggest that each of them has a significant impact on the required cooling. The most influential parameters are the cell temperature and the emitter temperature, and to a smaller extent, the view factor. Variations in emitter temperature, in-band and out-of-band transmission functions involve spectral behaviors and, as a result, impact differently the cells designed to maximize pairwise efficiency or to maximize power density. Depending on the objective (maximizing efficiency or power, or aiming for a balance between the two), selecting the optimal bandgap must

consider the cooling requirements and all other parameters influencing performance. In particular, making this bandgap selection by assuming that the cell operates in the radiative limit can be severely misleading. Although the thermal model is straightforward, involving the temperature of a cooler body and an effective heat transfer coefficient, the insights gained on the cooling requirements for thermophotovoltaic devices are significant. To meet these substantial cooling requirements, a thorough investigation into diverse technologies (including forced convection, phase change, two-dimensional spreaders, etc.) will undoubtedly be necessary. The electrical power potentially needed for cooling will have to be quantified and compared to the power produced by the cell. This power consumption is expected to vary depending on the type of cooling method and the design specific to each type (see the recent results involving liquid channels in [17]).

## CRediT authorship contribution statement

**Bhrigu Rishi Mishra:** Writing – original draft, Validation, Methodology, Investigation, Formal analysis. **Alexis Vossier:** Writing – review & editing, Validation, Formal analysis, Conceptualization. **Inès Revol:** Formal analysis, Conceptualization. **Guilhem Almuneau:** Writing – review & editing, Formal analysis, Conceptualization. **Rodolphe Vaillon:** Writing – review & editing, Validation, Supervision, Methodology, Investigation, Formal analysis, Conceptualization.

## Declaration of competing interest

The authors declare that they have no known competing financial interests or personal relationships that could have appeared to influence the work reported in this paper.

## Acknowledgments

This work was supported by Région Occitanie through the Défi-Clé PV-STAR (Photovoltaics in non-standard conditions).

## Data availability

Data will be made available on request.

## References

[1] T. Burger, C. Sempere, B. Roy-Layinde, A. Lenert, Present efficiencies and future opportunities in thermophotovoltaics, Joule 4 (2020) 1660–1680.
[2] A. Datas, R. Vaillon, Thermophotovoltaic energy conversion, in: Ultra-High Temperature Thermal Energy Storage, Transfer and Conversion, Elsevier, 2021, pp. 285–308.
[3] E.J. Tervo, R.M. France, D.J. Friedman, M.K. Arulanandam, R.R. King, T.C. Narayan, C. Luciano, D.P. Nizamian, B.A. Johnson, A.R. Young, et al., Efficient and scalable GaInAs thermophotovoltaic devices, Joule 6 (2022) 2566–2584.
[4] A. LaPotin, K.L. Schulte, M.A. Steiner, K. Buznitsky, C.C. Kelsall, D.J. Friedman, E.J. Tervo, R.M. France, M.R. Young, A. Rohskopf, et al., Thermophotovoltaic efficiency of 40%, Nature 604 (2022) 287–291.
[5] B. Roy-Layinde, J. Lim, C. Arneson, S.R. Forrest, A. Lenert, High-efficiency air-bridge thermophotovoltaic cells, Joule 8 (2024) 2135–2145.
[6] O. Dupré, R. Vaillon, M.A. Green, Optimization of solar thermophotovoltaic systems including the thermal balance, in: 2016 IEEE 43rd Photovoltaic Specialists Conference, PVSC, IEEE, 2016, pp. 1030–1033.
[7] E. Blandre, R. Vaillon, J. Drévillon, New insights into the thermal behavior and management of thermophotovoltaic systems, Opt. Express 27 (2019) 36340–36349.
[8] S. Shan, B. Chen, C. Shou, Parametric characteristics and optimization of a near-field thermophotovoltaic system considering cooling consumption, Sol. Energy 224 (2021) 629–636.
[9] M. Francoeur, R. Vaillon, M.P. Mengüç, Thermal impacts on the per- formance of nanoscale-gap thermophotovoltaic power generators, IEEE Trans. Energy Convers. 26 (2011) 686–698.
[10] J. DeSutter, M.P. Bernardi, M. Francoeur, Determination of thermal emission spectra maximizing thermophotovoltaic performance using a genetic algorithm, Energy Convers. Manage. 108 (2016) 429–438.
[11] B. Roux, C. Lucchesi, J.P. Perez, P.O. Chapuis, R. Vaillon, Main performance metrics of thermophotovoltaic devices: analyzing the state of the art, J. Photonics Energy 14 (2024) 042403–1.
[12] W. Shockley, H. Queisser, Detailed balance limit of efficiency of p–n junction solar cells, J. Appl. Phys. 32 (1961) 510–519.
[13] S. Rühle, Tabulated values of the Shockley–Queisser limit for single junction solar cells, Sol. Energy 130 (2016) 139–147.
[14] O. Dupré, R. Vaillon, M.A. Green, A full thermal model for photovoltaic devices, Sol. Energy 140 (2016) 73–82.
[15] O. Dupré, R. Vaillon, M.A. Green, Thermal behavior of photovoltaic devices, Phys. Eng. 10 (2017) 978–3.
[16] M.A. Green, A.W. Ho-Baillie, Pushing to the limit: radiative efficiencies of recent mainstream and emerging solar cells, ACS Energy Lett. 4 (2019) 1639–1644.
[17] H. Wang, M. Shimizu, R. Vaillon, D. Chemisana Villegas, O. Teixido, H. Yugami, Front-surface cooling of infrared thermophotovoltaic cells, Sol. Energy Mater. Sol. Cells 295 (2026) 113940.